

## Crustal deformation along the Altyn Tagh fault system, western China, from GPS

Zheng-Kang Shen,<sup>1</sup> Min Wang,<sup>2</sup> Yanxing Li,<sup>2</sup> David D. Jackson,<sup>1</sup> An Yin,<sup>1</sup> Danan Dong,<sup>3</sup> and Peng Fang<sup>4</sup>

**Abstract.** We collected GPS data from the southern Tarim basin, the Qaidam basin, and the western Kunlun Shan region between 1993 and 1998 to determine crustal deformation along the Altyn Tagh fault system at the northern margin of the Tibetan plateau. We conclude from these data that the Altyn Tagh is a left-lateral strike slip fault with a current slip rate of  $\sim 9$  mm/yr, in sharp contrast with geological estimates of 20–30 mm/yr. This contrast poses an enigma: because the GPS data cover a wider region than the geologic data, they might be expected to reveal somewhat more slip. We also find that the Tarim and Qaidam basins behave as rigid blocks within the uncertainty of our measurements, rotating clockwise at a rate of  $\sim 11$  and  $\sim 4.5$  nrad/yr, respectively, with respect to the Eurasia plate. The rotation of the Tarim basin causes convergence across the Tian Shan, increasing progressively westward from  $\sim 6$  mm/yr at  $87^\circ\text{E}$  to  $\sim 18$  mm/yr at  $77^\circ\text{E}$ . Our data and other GPS data suggest that the Indo-Asia collision is mainly accommodated by crustal shortening along the main Himalayan thrust system ( $\sim 53\%$ ) and the Tian Shan contractional belt ( $\sim 19\%$ ). Eastward extrusion of the Tibetan plateau along the Altyn Tagh and Kunlun faults accommodates only  $\sim 23\%$  of the Indo-Asia convergence.

### 1. Introduction

In the past decades, two end-member models have emerged to characterize the mechanical behavior of continental deformation. In one view, the continents undergo distributed deformation [e.g., Bird and Piper, 1981; England and Houseman, 1986; Houseman and England, 1996; Royden et al., 1997; Holt et al., 1995, 2000]. In another view, continents deform as a collage of rigid blocks whose motions may be described by the same rules so successfully applied to the kinematics of oceanic plates (e.g., see Weldon and Humphreys [1986] for the San Andreas system, Wernicke et al. [1988] for the Basin and Range extensional system, and Avouac and Tapponnier [1993] for the Indo-Asian collision zone). These contrasting views on the behavior of continental deformation are best exemplified by the two well-known hypotheses for Cenozoic deformation of Asia due to the Indo-Asian collision: (1) distributed crustal thickening [Dewey and Burke, 1973; England and Houseman, 1986] and (2) lateral extrusion [Tapponnier et al., 1982; Peltzer and Tapponnier, 1988]. The first emphasizes the role of distributed thrusts and folds in absorbing north-south shortening and implies weak continental lithosphere, widespread deformation, and slow slip rates along strike-slip faults. The second suggests large-scale ( $\sim 1000$  km) eastward translation of continental blocks and

implies strong continental lithosphere, plate-like movements and fast rates along strike-slip faults. Modeling attempts have been made to reconcile the two [Kong and Bird, 1996; Peltzer and Saucier, 1996], but the uncertainties are large because of limited data constraints. Geologically, the two models may be differentiated by determining the fault kinematics and the total magnitude of fault slip in the Indo-Asian collision zone [e.g., Leloup et al., 1995; Yin and Harrison, 2000]. Alternatively, the models can be tested directly by GPS studies, which effectively determine current rates of deformation [Abdrakhmatov et al., 1996; Bilham et al., 1997; King et al., 1997; Zhu et al., 2000; Larson et al., 1999; Chen et al., 2000; Shen et al., 2000]. For example, GPS studies can test if major strike-slip faults like the Altyn Tagh, the eastern Kunlun, and the Karakoram move at fast rates ( $>10$  mm/yr) and if individual blocks bounded by these faults simply rotate about a few Euler poles, as predicted by the lateral extrusion tectonic model [Avouac and Tapponnier, 1993]. Our study provides one of such tests along the Altyn Tagh fault system.

### 2. Geologic Setting

The northern margin of the Tibetan plateau is defined by the Altyn Tagh fault system, which consists of the  $\sim 1200$  km long, ENE trending Altyn Tagh fault in the middle and the WNW trending western Kunlun and Nan Shan thrust belts at its two ends [Molnar and Tapponnier, 1975; Yin and Harrison, 2000] (Figure 1). The active trace of the Altyn Tagh fault is a well-defined morphologic feature between  $85^\circ$  and  $95^\circ\text{E}$  [Peltzer et al., 1989]. West of  $85^\circ\text{E}$  the Altyn Tagh fault splits into three segments: (1) the western Kunlun thrust system, which lies nearly perpendicular to the main trace of the Altyn Tagh fault and bounds the westernmost Tibetan plateau to the south and the Tarim basin to the north, (2) the left slip Karakash fault parallel to the western Kunlun thrust system along the southern edge of the western Kunlun Shan, and (3) several left stepping splays of left slip faults and small pull-

<sup>1</sup>Department of Earth and Space Sciences, University of California, Los Angeles, California, USA.

<sup>2</sup>First Crustal Deformation Monitoring Center, China Seismological Bureau, Tianjin, China.

<sup>3</sup>Jet Propulsion Laboratory, Pasadena, California, USA.

<sup>4</sup>Scripps Orbit and Permanent Array Center (SOPAC), Cecil H. and Ida M. Green Institute of Geophysics and Planetary Physics, Scripps Institution of Oceanography, La Jolla, California, USA.

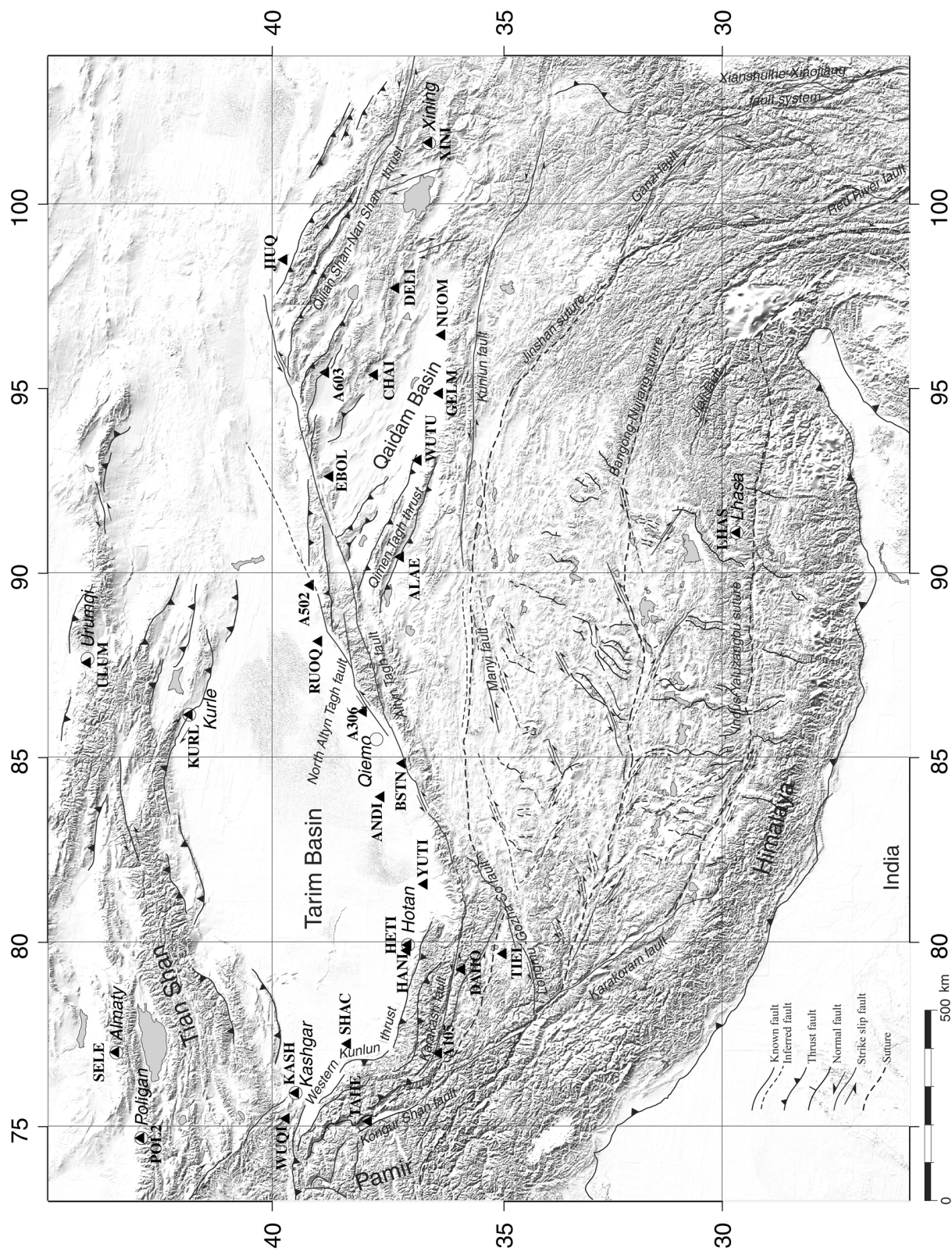


**Figure 1.** Active tectonic setting in western China and central Asia (modified after Taylor et al. (submitted manuscript, 2001)). Triangles are the GPS stations used in this study. Open circles denote the locations of the cities.

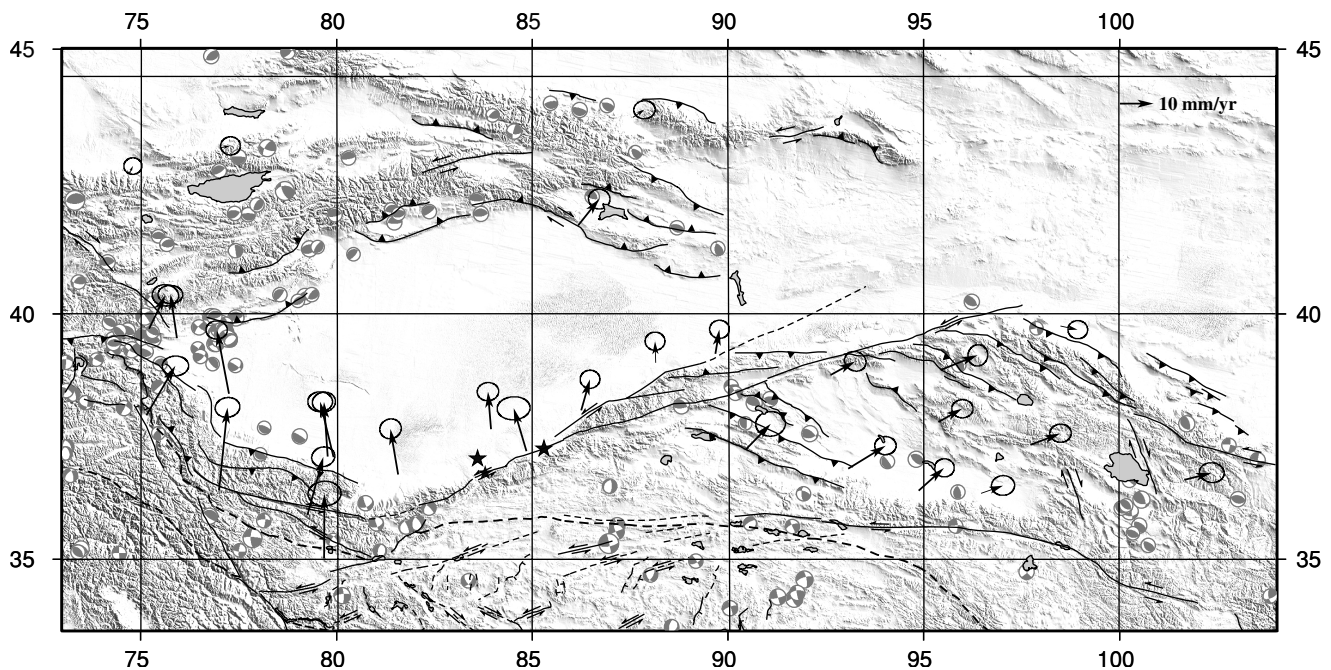


**Figure 2.** GPS velocities with respect to the Eurasia fixed reference frame. GPS solutions were derived using NUVEL-1A model constraints. Each velocity arrow originates at the location of the site and points to its motion direction. The error ellipses represent 95% confidence. The earthquake focal mechanisms are from the Harvard centroid moment tensor (CMT) catalog, 1976–1999. Stars are the  $M > 6$  historical earthquakes occurred along the Altyn Tagh fault.

apart basins (i.e., the Longmu-Gozha Co fault system, Figure 1) along the southwestward projection of the main trace of the Altyn Tagh fault [State Seismological Bureau of China (SSBC), 1992; Avouac and Peltzer, 1993]. East of 95°E the Altyn Tagh fault links with the ~400 km wide Qilian Shan-Nan Shan thrust belt [Burchfiel et al., 1989; Tapponnier et al., 1990; Meyer et al., 1998].

Directly north of the central Altyn Tagh fault between 87° and 93°E lies the Altyn Tagh range. Its northern rim is locally bounded by active fault traces that have been inferred to represent a thrust system accommodating shortening perpendicular to the Altyn Tagh fault [Burchfiel et al., 1989; Tapponnier et al., 1990]. Recent field mapping suggested that the range-bounding fault is an oblique left slip system that has only a minor component of north-south shortening [Cowgill et al., 2000]. North of the Altyn Tagh range is the Tarim basin, largely overlain by Quaternary sediments. The Tarim basin is bounded to the north by the southern Tian Shan thrust belt [Yin et al., 1998].

Toward the western end of the fault system a seismic reflection profile across the western Kunlun thrust belt showed a gentle south dip of the Moho beneath the Tarim north of the fault, suggesting that the Tarim has underthrust the Kunlun Mountains [Kao et al., 1999]. Such an interpretation is also consistent with the regional gravity data [Lyon-Caen and Molnar, 1984; Jiang et al., 1999]. About 5 mm/yr convergence was inferred on structures within the western Kunlun thrust belt [Avouac and Peltzer, 1993]. However, earthquake data demonstrated active east-west normal faulting south of the Karakash fault in northern Tibet, showing a strain pattern of east-west extension [Molnar and Lyon-Caen, 1989].

In the Qaidam basin south of the Altyn Tagh fault, folded Quaternary strata are widely distributed which trend at a high angle to the Altyn Tagh fault. No obvious bending of the fold axes is apparent, suggesting that left slip shear between the Tarim

and Qaidam blocks has been concentrated along the narrow Altyn Tagh fault alone [Yin and Harrison, 2000]. In contrast, several folds appear to exist southwest of the Qaidam basin in the westernmost end of the Qimen Tagh, implying that a fraction of shear deformation associated with the Altyn Tagh fault may splay into a zone of transpressional deformation [Yin and Harrison, 2000].

The Altyn Tagh fault is seismically active. Two large earthquakes (both inferred to be  $M = 7.2$ ) occurred west of Qiemo along the fault in 1924 [Abe, 1984; SSBC, 1992]. In 1933, another earthquake of  $M = 6.7$  occurred along the fault south of Qiemo [SSBC, 1992] (Figure 2). However, contemporary instrumental recordings revealed only a minor level of seismicity along the entire fault system. The seismicity maps of Ma [1989] and SSBC [1992] showed that numerous  $M = 5-6$  earthquakes occurred in the Qaidam basin from mid-1960s to early 1990s, mostly within the Qimen Tagh thrust system and in the region south of Qinghai Lake. The largest earthquake in the region was an  $M = 7.6$  left slip event (the Manyi earthquake) in 1997 along a nearly east-west trending fault at the eastern termination region of the Kunlun fault [Peltzer et al., 1999] (Figure 2).

### 3. GPS Data Collection and Analysis

GPS experiments were conducted along the northern margin of Tibet and the southern Tarim basin on both sides of the Altyn Tagh system by Chinese survey teams in 1993, 1994, 1996, and 1997 and by a joint UCLA-China survey team in 1998 (Figure 1). A total of 25 stations were occupied for 2–5 days during each experiment, with 8–24 hours of data collected each day (Table 1). Two stations located on both the northern and southern ends of the eastern Tian Shan (ULUM and KURL) were

**Table 1.** Station Occupation History<sup>a</sup>

Site	93.2 <sup>b</sup>	94.6 <sup>b</sup>	96.5 <sup>b</sup>	97.2 <sup>b</sup>	98.4 <sup>b</sup>
KURL	MIN	LEI	ASH	nd <sup>c</sup>	nd
RUOQ	MIN	LEI	LEI	ASH	ROG
HETI	MIN	nd	nd	ASH	ROG
A105	MIN	nd	nd	ASH	ROG
DAHO	MIN	nd	nd	ASH	ROG
TIEL	nd	nd	nd	ASH	ROG
ALAE	nd	nd	nd	ASH	ROG
TAHE	MIN	nd	nd	nd	ROG
WUTU	MIN	nd	nd	ASH	ROG
A306	MIN	nd	nd	ASH	ROG
ANDI	MIN	nd	nd	ASH	ROG
WUQI	MIN	nd	nd	nd	ROG
YUTI	MIN	nd	nd	ASH	ROG
A502	MIN	nd	nd	nd	ROG
A603	MIN	nd	nd	nd	ROG
EBOL	MIN	nd	nd	nd	ROG
BSTN	nd	nd	nd	ASH	ROG
CHAI	LEI	nd	nd	ASH	ROG
DELI	LEI	nd	nd	ASH	ROG
NUOM	MIN	nd	nd	ASH	nd
GLM1 <sup>d</sup>	MIN	nd	nd	ASH	nd
GELM <sup>d</sup>	LEI	LEI	LEI	ASH	ROG
JIUQ	LEI	LEI	LEI	nd	ROG
KASH	nd	LEI	ASH	nd	ROG
SHAC	nd	LEI	nd	nd	ROG
HANI	nd	LEI	ASH	nd	nd
ULUM	nd	LEI	ASH	nd	nd
XINI	nd	LEI	LEI	nd	nd

<sup>a</sup>Receiver/antenna units used: MIN, MinMac; LEI, Leica; ASH, Ashtech Z12; ROG, Rogue.

<sup>b</sup>Here columns 93.2 to 98.4 refer to occupation time epochs; 93.2 means year 1993.2, which is around March in 1993.

<sup>c</sup>Here nd means no data were collected at that time epoch.

<sup>d</sup>Stations located ~5 km apart; their velocities are tied together.

measured during the same time period and are also included in this study. These stations are either installed on bedrock or buried in sediments. For the latter, the monuments are composed of a large block of concrete buried ~3 m below the surface with its survey marker projected in a pit at a depth of ~1 m. The burial installation of the markers reduced the surface perturbation. See Table 1 for a detailed site occupation history.

We processed the GPS data in three steps. First, all the survey mode data collected in the Altyn Tagh region were processed together with the data collected from regional IGS tracking stations in Asia using the GAMIT software [King and Bock, 1995]. The phase data were modeled to solve for parameters such as station positions, satellite orbits, polar motions, and atmospheric delay corrections. A loosely constrained solution for the station positions was obtained for each day. In the next step we combined the regional daily solutions with the global solutions of ~60 tracking sites produced at the Scripps Orbital and Position Analysis Center (SOPAC [Bock et al., 1997]) using the GLOBK software [Herring, 1995]. Common parameters in both solutions, such as the satellite orbits, polar motions, and tracking station positions, were solved with loose constraints on all the parameters. In the last step we estimated station positions and velocities using the QOCA software [Dong et al., 1998] (also see <http://gipsy.jpl.nasa.gov/qoca>). To strengthen the solutions at the global tracking sites, we also added about a month of the SOPAC global solutions each year for 1992, 1995, 1999, and 2000, during which no regional data were collected. The QOCA modeling of the data was done through sequential Kalman filtering, allowing adjustment for global translation and rotation of each daily solution. Random walk style perturbations were allowed for some parameters whose errors were found correlated with time (e.g., the

Earth's rotation parameters and the antenna heights at a few sites). For more details about the data analysis procedure and uncertainty estimation, please refer to Shen et al. [2000] and <http://gipsy.jpl.nasa.gov/qoca>.

As shown in Table 1, our stations were measured using various manufactures of GPS receiver/antenna units. For some of the antenna units, such as the Dorn/Margolin and MiniMac, the physical locations of the phase centers are either known to be precise to the manufacture specifications or have been well mapped and modeled subsequently in the GAMIT data processing. For the Ashtech and Leica units, we know that their phase center locations may be shifted, but we have no precise information to quantify this shift. We therefore allowed phase center shifts for those antenna types to be estimated during QOCA modeling, adding six degrees of freedom (three for each antenna type) to the parameter space in our solution. The resolved shifts for the east, north, and up components are  $-1.1 \pm 1.0$ ,  $-6.4 \pm 0.5$ , and  $13.7 \pm 12.7$  mm for Leica and  $-3.0 \pm 0.8$ ,  $-11.2 \pm 0.4$ , and  $21.2 \pm 10.1$  mm for Ashtech Z12 antennae, respectively. The phase center shift estimate for Ashtech Z12 antennae agrees with our unpublished results using data collected with the same receiver/antenna units from different experiments. Figure 3 shows the postfit time series of the regional sites, with antenna phase center shifts marked by small jumps in some of the model prediction curves.

In the last step we also tied the velocity solution to a reference frame fixed to the Eurasia plate. How this might be best achieved has been a subject of discussion [Shen et al., 2000; Kogan et al., 2000]. We used two approaches considered to be robust and relatively unbiased. The first (named "NUVEL-1A") links our result to model predictions of the no net rotation (NNR) NUVEL-1A [DeMets et al., 1990; 1994; Argus and Gordon, 1991]. Velocities at nine global tracking stations located at the stable interiors of Eurasia, North and South America, Australia, Africa, and Antarctica were constrained to their NNR NUVEL-1A values with the uncertainties of 2, 2, and 4 mm/yr for the east, north, and up components, respectively. These stations were selected because of their long tracking history and their proven consistency with the NUVEL-1A model [Larson et al., 1997]. By adopting this approach, our velocity solution was referenced to the stable part of the Eurasia plate. The reference is not defined merely by the sites located in northern and western Europe but by a group of globally located stations in the stable interiors of several continents (see Shen et al. [2000] for a more detailed discussion of the approach).

The second approach we used (named "EURASIA") ties the velocity results to a geodetically determined Eurasian plate reference frame. This approach is similar to that of Kogan et al. [2000] and Chen et al. [2000]. We first used the geodetic model of International Terrestrial Reference Frame (ITRF97) [Sillard et al., 1998] (see also <http://lareg.ensg.ign.fr/ITRF/ITRF97>) to constrain our solution. We chose as our reference stations those whose formal ITRF97 velocity uncertainties are <0.5 mm/yr. We then linked our velocities at the sites to their ITRF97 values with uncertainties of 2, 2, and 4 mm/yr for the east, north, and up components, respectively. The purpose of doing so was to better integrate the regional solutions with a well-defined global reference frame. This is especially important for the early years data, when the International GPS Service (IGS) network coverage was quite thin in east Asia. In the next step we rotated the solution to a Eurasia fixed reference frame by minimizing the velocity RMS at a number of sites located in Siberia, western and northern Europe, and Svalbard Island in the Arctic Ocean. All these sites are believed to be in the stable part of the Eurasia plate. We started with 18 such stations and estimated the rotation parameters iteratively: in each step removing from the least squares adjustment a site with the largest postfit residual of the horizontal velocity components. The iteration was stopped when all postfit residuals of the horizontal

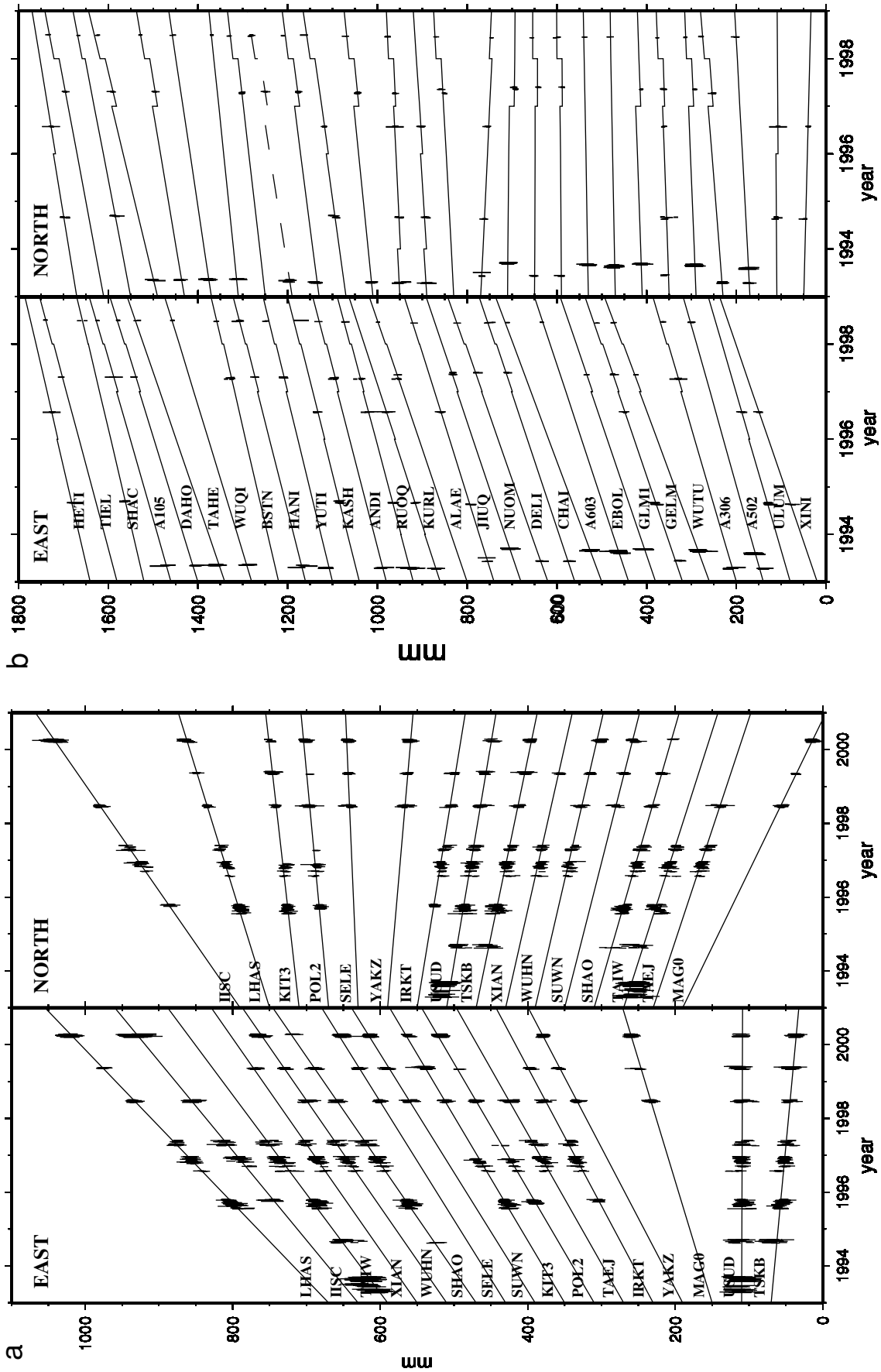
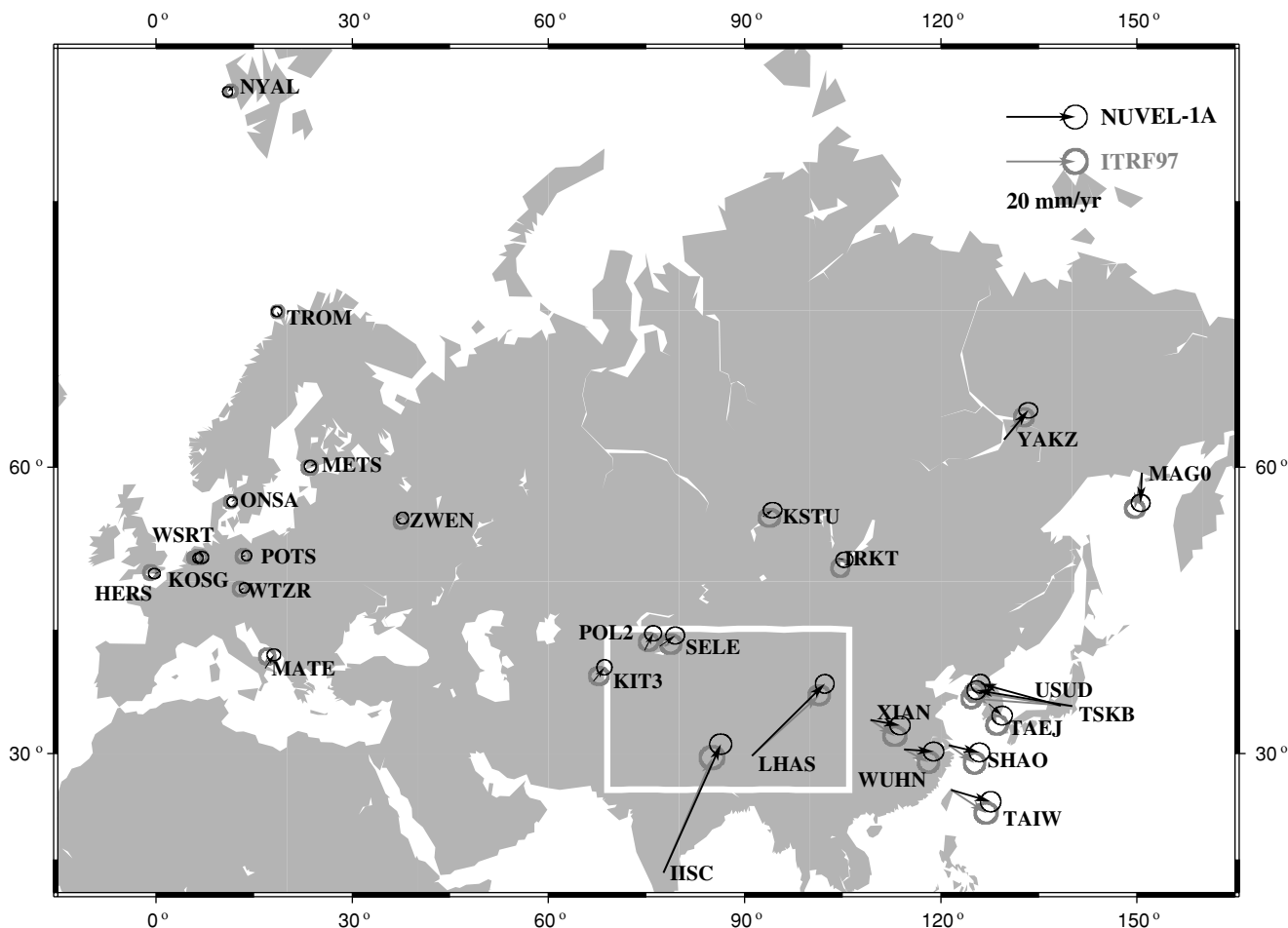


Figure 3. Time series of station positions. Data are shown with  $1\sigma$  standard deviation. The solid lines are postfit model predictions. (a) IGS sites in Asia and (b) the Altyn Tagh campaign mode sites. Kinks in the prediction curves represent jumps induced by receiver/antenna changes.



**Figure 4.** Eurasian and Indian IGS station velocities with respect to the Eurasia plate. Solid arrows are solutions constrained to the NUVEL-1A, and shaded arrows are solutions to the EURASIA reference frames. The white rectangle highlights the region to be studied.

velocity components at the sites were  $< 2$  mm/yr. Of the 18 stations, 13 survived the process to become the reference sites of the Eurasia plate (Figure 4). Although this approach used ITRF97 velocities as the initial constraints for some of the IGS stations, our final reference frame is not defined by the ITRF97 frame but by the binding of IGS sites in the stable part of the Eurasia plate.

Both approaches have advantages and weaknesses. The NUVEL-1A approach relies on the global strength of the NUVEL-1A model. However, the model might be biased if used to constrain contemporary deformation because it is based on data averaged over geological time. Such biases can be propagated into the reference frame. Conversely, realization of the Eurasian reference frame for our EURASIA solution relies heavily on two IGS sites: KSTU and IRKT in Siberia. For the other two Siberian IGS sites, YAKZ is not stable enough to be used as a reference, and MAG0 is probably located at the North American plate [Kogan *et al.*, 2000]. KSTU has a relatively short occupation history ( $\sim 2$  years), and it is not clear if IRKT is affected by rifting around Lake Baikal. In spite of these concerns, the two reference frames are quite close, and they differ only by a rigid body rotation of  $0.55$  nrad/yr, around a rotation pole at  $16.0^\circ\text{E}$ ,  $57.4^\circ\text{N}$ . The most significant discrepancies between the two solutions come from sites in easternmost Asia and India:  $\sim 3.4$  mm/yr in the NNE direction. Here we

provide the velocity solution in both reference frames (Table 2) but show only the NUVEL-1A solution in the figures of regional deformation.

#### 4. Results

Figure 2 shows the velocity solutions in the Altyn Tagh region with respect to the stable Eurasia plate. The first-order features are the clockwise rotation of the Tarim basin and left slip motion along the Altyn Tagh fault. In particular, Tarim rotates clockwise with respect to Siberia at a rate of  $10.8 \pm 0.8$  nrad/yr around a pole at  $36.0^\circ \pm 0.4^\circ\text{N}$  and  $99.1^\circ \pm 0.8^\circ\text{E}$  (Figure 5), estimated from fitting the NUVEL-1A referenced station velocities of 10 sites (SHAC, HANI, HETI, YUTI, ANDI, BSTN, A306, RUOQ, A502, and JIUQ) along the southern rim and one site (KURL) near the northern rim of Tarim (Table 3). If the EURASIA station velocities are used, the rotation rate is  $11.1 \pm 0.8$  nrad/yr around a pole at  $37.5^\circ \pm 0.4^\circ\text{N}$  and  $96.2^\circ \pm 0.8^\circ\text{E}$  (Figure 4). The two rotation poles are  $\sim 280$  km apart from each other, which reflects the systematic difference of the NUVEL-1A and EURASIA reference systems. The Qaidam-Kunlun Shan block, delineated by the Altyn Tagh fault and the Nan Shan-Qilian Shan thrust belt to the north and the Kunlun fault to the south, rotates counterclockwise at a rate  $7.0 \pm 1.7$  nrad/yr around a pole of  $48.3^\circ \pm 2.3^\circ\text{N}$ ,  $88.0^\circ \pm 1.5^\circ\text{E}$  with

**Table 2.** Station Velocities<sup>a</sup>

SITE	Longitude, °E	Latitude, °N	East, mm/yr					North, mm/yr					σ	Corr
			EURA	GPS EURA	NUVEL	GPS NUVEL	σ	URA	GPS EURA	NUVEL	GPS NUVEL			
<i>IGS Station Velocities</i>														
HERS	0.336	50.867	16.9	-2.2	17.4	-1.1	0.7	14.8	0.0	15.0	-0.3	0.6	0.00	
KOSG	5.810	52.178	17.6	0.2	18.2	1.2	0.6	14.6	0.3	14.3	0.2	0.6	0.01	
WSRT	6.604	52.915	17.6	-0.1	18.2	0.8	0.8	14.5	-1.8	14.2	-1.9	0.7	0.02	
NYAL	11.865	78.930	9.5	-0.7	12.8	-1.7	0.6	14.1	-1.3	13.4	-1.5	0.6	-0.01	
ONSA	11.925	57.395	17.3	-1.0	18.4	-0.5	0.6	14.1	-0.6	13.4	-0.6	0.6	0.01	
WTZR	12.879	49.144	19.9	0.0	20.0	1.2	0.6	14.0	0.3	13.2	0.6	0.6	0.02	
POTS	13.066	52.379	19.0	0.5	19.5	1.5	0.6	14.0	0.1	13.2	0.3	0.6	0.01	
MATE	16.704	40.649	22.5	0.6	21.7	2.5	0.8	13.7	3.3	12.6	3.9	0.7	0.00	
TROM	18.938	69.663	14.6	-0.6	16.9	-0.9	0.6	13.4	1.5	12.2	1.6	0.6	0.00	
METS	24.395	60.218	18.9	-1.7	20.1	-1.5	0.7	12.7	-1.0	11.1	-0.6	0.7	-0.01	
ZWEN	36.759	55.699	22.3	1.3	22.7	1.8	0.7	10.8	-0.5	8.3	0.5	0.7	0.02	
KIT3	66.885	39.135	28.0	1.6	25.6	3.2	0.9	4.1	1.5	0.2	4.0	0.9	0.01	
POL2	74.694	42.680	28.0	1.2	25.5	2.5	1.0	2.1	2.5	-2.0	5.0	0.9	0.01	
SELE	77.017	43.179	28.0	3.2	25.4	4.5	1.1	1.5	0.6	-2.7	3.1	1.0	0.01	
IISC	77.570	13.021	27.1	14.1	39.7	-0.2	1.3	1.4	33.3	41.1	-6.7	1.2	-0.00	
LHAS	91.104	29.657	28.5	19.5	24.6	21.1	1.1	-2.1	17.6	-6.5	20.9	1.1	0.01	
KSTU	92.794	55.993	25.9	1.9	23.2	2.8	1.1	-2.6	-0.4	-6.9	1.8	0.9	0.01	
IRKT	104.316	52.219	26.0	0.6	22.4	1.8	1.0	-5.4	-2.8	-9.7	-0.4	0.9	0.01	
XIAN	109.222	34.369	27.7	7.1	23.2	8.6	1.2	-6.6	-4.7	-10.8	-1.6	1.1	0.01	
WUHN	114.357	30.532	27.5	7.1	22.7	8.6	1.2	-7.8	-3.7	-11.8	-0.6	1.1	0.00	
SHAO	121.200	31.100	27.0	7.5	21.9	8.9	1.2	-9.3	-5.2	-13.1	-2.1	1.1	0.00	
TAIW	121.537	25.021	27.1	10.2	22.0	11.5	1.2	-9.3	-6.7	-13.1	-3.4	1.2	0.00	
TAEJ	127.366	36.374	26.0	2.3	20.8	3.8	1.2	-10.5	-6.1	-14.0	-3.4	1.1	0.01	
YAKZ	129.681	62.031	20.5	5.7	16.0	7.0	1.1	-10.9	6.5	-14.3	8.5	0.9	-0.02	
USUD	138.362	36.133	24.7	-24.9	19.1	-23.3	1.1	-12.3	3.9	-15.3	6.4	1.1	0.01	
TSKB	140.088	36.106	24.5	-29.2	18.9	-27.7	1.1	-12.6	2.2	-15.5	4.6	1.1	0.01	
MAGO	150.770	59.576	17.2	-2.1	11.7	-0.4	1.1	-13.8	-10.5	-16.1	-8.8	1.0	-0.02	
<i>Regional Station Velocities</i>														
TAHE	75.145	37.971	28.4	7.9	25.5	9.4	1.4	2.0	13.8	-2.1	16.4	1.1	0.09	
WUQI	75.217	39.705	28.2	4.1	25.5	5.5	1.4	2.0	8.9	-2.2	11.5	1.1	0.00	
KASH	75.920	39.517	28.3	-1.8	25.5	-0.3	1.4	1.8	13.0	-2.3	15.5	1.1	-0.01	
A105	77.001	36.444	28.5	1.9	25.4	3.5	1.4	1.5	24.0	-2.7	26.8	1.1	0.15	
SHAC	77.248	38.412	28.4	-3.6	25.4	-2.0	1.2	1.5	18.8	-2.7	21.5	1.0	-0.00	
DAHO	79.257	35.937	28.5	4.2	25.3	5.9	1.3	1.0	16.8	-3.3	19.7	1.1	0.14	
TIEL	79.685	35.026	28.6	-0.2	25.3	1.4	1.9	0.8	19.0	-3.4	21.9	1.5	0.04	
HANI	79.774	37.135	28.5	-1.6	25.3	0.0	1.3	0.8	15.7	-3.4	18.5	1.0	0.10	
HETI	79.926	37.121	28.5	-3.9	25.3	-2.3	1.4	0.8	16.5	-3.5	19.4	1.1	-0.01	
YUTI	81.577	36.765	28.5	-2.7	25.3	-1.1	1.2	0.4	13.3	-3.9	16.2	1.1	0.10	
ANDI	83.945	37.696	28.5	-1.2	25.2	0.3	1.2	-0.3	10.9	-4.6	13.8	1.0	0.05	
BSTN	84.850	37.242	28.5	-3.9	25.1	-2.3	1.9	-0.5	12.6	-4.8	15.5	1.4	0.05	
KURL	86.169	41.708	28.1	6.3	25.0	7.7	1.3	-0.8	7.7	-5.2	10.4	1.1	-0.02	
A306	86.251	38.077	28.4	2.6	25.0	4.1	1.2	-0.9	9.2	-5.2	12.0	1.0	0.02	
ULUM	87.574	43.745	27.9	3.4	24.8	4.8	1.2	-1.2	2.3	-5.5	4.9	1.0	0.02	
RUOQ	88.153	39.029	28.3	-0.1	24.9	1.4	1.1	-1.4	6.4	-5.7	9.2	1.0	0.00	
A502	89.680	39.205	28.3	1.4	24.8	2.9	1.2	-1.8	7.4	-6.1	10.2	1.0	0.00	
ALAE	90.442	37.274	28.4	7.5	24.8	9.0	1.8	-2.0	7.6	-6.3	10.5	1.4	0.02	
EBOL	92.624	38.790	28.3	6.8	24.6	8.3	1.3	-2.5	4.5	-6.9	7.4	1.1	-0.10	
WUTU	93.067	36.890	28.4	10.6	24.6	12.1	1.3	-2.6	6.8	-7.0	9.8	1.1	0.01	
GELM	94.874	36.433	28.3	7.7	24.5	9.2	1.2	-3.1	6.8	-7.4	9.7	1.0	0.01	
CHAI	95.377	37.834	28.2	7.1	24.4	8.7	1.2	-3.2	4.0	-7.6	6.9	1.1	0.01	
A603	95.436	38.881	28.2	11.3	24.4	12.7	1.2	-3.2	5.1	-7.6	8.0	1.1	0.03	
NUOM	96.458	36.381	28.3	7.5	24.4	8.9	1.3	-3.5	2.6	-7.8	5.5	1.1	0.01	
DELI	97.730	37.377	28.2	8.9	24.2	10.4	1.2	-3.8	3.4	-8.2	6.4	1.1	0.01	
JIUQ	98.496	39.758	28.0	5.2	24.1	6.6	1.2	-4.0	-1.1	-8.3	1.8	1.0	0.00	
XINI	101.654	36.660	28.0	8.2	24.1	9.5	1.4	-4.8	2.1	-8.7	4.7	1.1	-0.06	

<sup>a</sup>EURA, a priori velocity in EURASIA reference frame; NUVEL, a priori velocity in NUVEL-1A reference frame; GPS, velocity increment with respect to the reference frame shown in previous column; σ, one standard deviation uncertainty; Corr, velocity correlation between the east and north components.

respect to the Tarim basin, estimated from velocities of nine stations (ALAE, EBOL, WUTU, GELM, CHAI, A603, NUOM, DELI, and XINI) within the basin (Figure 6). Our GPS results detect little deformation within the Tarim and Qaidam-Kunlun Shan blocks (Figures 5 and 6). Rotation postfit residuals for the Tarim basin sites are 1.7 and 1.1 mm/yr for the east and north

components, respectively. The postfit residuals for the Qaidam-Kunlun Shan sites are 1.5 and 1.1 mm/yr for the east and north velocity components. Such residuals are within the error range of the data, suggesting negligible deformation within both blocks.

South of the Altyn Tagh fault the Qaidam-Kunlun Shan block moves eastward as a coherent unit with respect to the Tarim

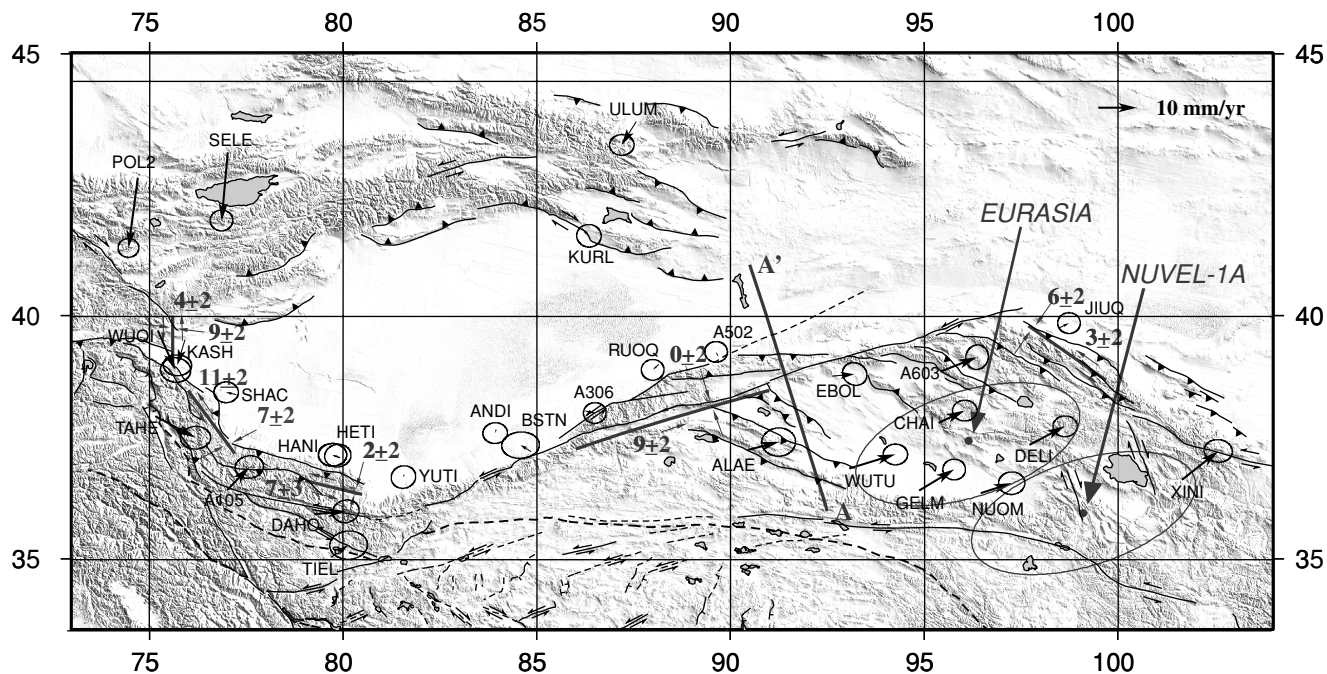


**Figure 5.** Close-up view of regional station velocities with respect to the Tarim basin. A rigid-body rotation of the Tarim basin with respect to Siberia has been removed from all the station velocities. Two rotation poles of Tarim with respect to Siberia are shown, one for the EURASIA and the other for the NUVEL-1A referenced solutions, respectively. Error ellipses are 95% confidence. Slip rates across several fault segments are shown. The thick straight lines along faults mark the strike directions along which the slip rates are measured.

basin. Along the central section of the Altyn Tagh fault, we determine  $9 \pm 2$  mm/yr left slip and  $0 \pm 2$  mm/yr convergence across the fault, measured between a group of three stations (A502, RUOQ, and A306) located north and west of the Altyn Tagh range and another group of eight stations (ALAE, EBOL, WUTU, A603, CHAI, GELM, DELI, and NUOM) in the central and western Qaidam basin (Figure 5). Close to the Altyn Tagh fault, however, a station velocity profile across the surface fault trace shows distributed shear deformation over a 150–200 km wide zone (Figure 7). Shear deformation across both the Altyn Tagh and the North Altyn Tagh faults is too broad to be accounted for by the elastic strain distribution of the Altyn Tagh fault alone, implying that both faults are slipping at depth and locked at the surface.

The clockwise rotation of the Tarim basin results in greater north-south shortening for the central western Tian Shan than for the eastern Tian Shan. Our result places  $18 \pm 2$  mm/yr north-south convergence at  $\sim 77^\circ\text{E}$  between SELE, located north of the Tian Shan, and SHAC southwest of the Tarim basin. Because the two stations span the entire range of the Tian Shan belt, this result indicates the total shortening rate across the Tian Shan range. It is consistent with an estimate of 13 mm/yr shortening

across a GPS network covering the northern two thirds of the Tian Shan belt [Abdrakhmatov *et al.*, 1996]. To the east the shortening across the Tian Shan between ULUM and KURL at  $\sim 87^\circ\text{E}$  is  $6 \pm 2$  mm/yr, significantly smaller than its western counterpart. Our data indicate little east-west shear motion across the Tian Shan belt.

At the western end of the Altyn Tagh fault system the Karakash fault in the western Kunlun Shan slips left laterally at a rate of  $7 \pm 3$  mm/yr, determined from station velocities of four sites (HANI, HETI, DAHO, and TIEL) located across the fault. In addition, a convergence rate of  $2 \pm 2$  mm/yr in the direction of  $\text{N}10^\circ\text{E}$  is detected across the eastern segment of the western Kunlun thrust belt. Both the left slip rate along the Karakash fault and convergence rate across the western Kunlun thrust belt increase westward. This is shown as a  $7 \pm 2$  mm/yr convergence in the direction of  $\text{N}50^\circ\text{E}$  between SHAC and TAHE, some 180 km apart from each other across the thrust. A left slip rate of  $11 \pm 2$  mm/yr is also detected between the two stations parallel to the western Kunlun Shan trending  $\text{N}40^\circ\text{W}$ .

Our GPS measurements also detect significant deformation at the western end of the southern Tian Shan thrust belt [Yin *et al.*, 1998]. Station KASH at town Kashgar moves southward with

**Table 3.** Basin Rotation Rates

Reference	Tarim With Respect to Siberia			Qaidam With Respect to Siberia			Qaidam With Respect to Tarim		
	Rotation Rate, nrad/yr	Longitude, $^\circ\text{E}$	Latitude, $^\circ\text{N}$	Rotation Rate, nrad/yr	Longitude, $^\circ\text{E}$	Latitude, $^\circ\text{N}$	Rotation Rate, nrad/yr	Longitude, $^\circ\text{E}$	Latitude, $^\circ\text{N}$
NUVEL-1A	$10.8 \pm 0.8$	$99.1 \pm 0.8$	$36.0 \pm 0.4$	$4.4 \pm 1.4$	$111.2 \pm 2.5$	$14.7 \pm 5.4$	$-7.0 \pm 1.7$	$88.0 \pm 1.6$	$48.3 \pm 2.3$
EURASIA	$11.1 \pm 0.8$	$96.2 \pm 0.8$	$37.5 \pm 0.4$	$4.6 \pm 1.4$	$105.2 \pm 2.5$	$19.9 \pm 5.5$	$-6.9 \pm 1.6$	$87.5 \pm 1.5$	$48.6 \pm 2.3$

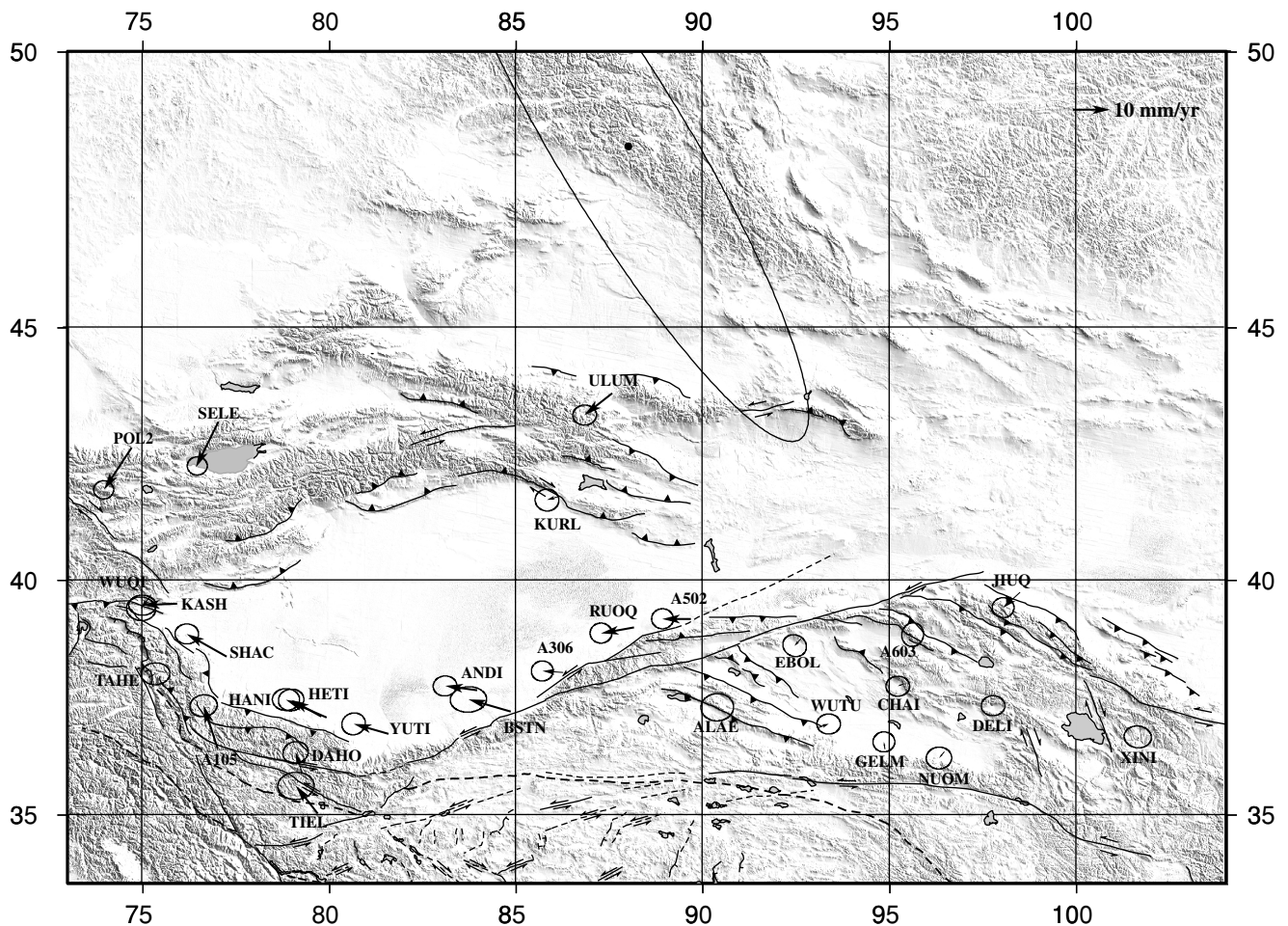


**Figure 6.** Close-up view of regional station velocities with respect to the Qaidam basin. A rigid-body rotation of the Qaidam basin with respect to Siberia has been removed from all station velocities. A rotation pole of the Qaidam basin with respect to the Tarim basin is shown. Its error ellipse represents 95% confidence.

respect to the Tarim block (defined by all the stations within the basin except KASH) at a rate of  $7 \pm 2$  mm/yr (Figure 5). This motion shows that the westernmost tip of the Tarim basin should be part of the southern Tian Shan thrust system [Yin *et al.*, 1998; Allen *et al.*, 1999; Burchfiel *et al.*, 1999] and is being detached from the rest of the basin. Or possibly the southern frontal thrust fault of Tian Shan immediately north of the site is locked and a considerable amount of seismic moment is accumulating as elastic strain. In either case, its active tectonics agrees with the active seismicity in the Jiashi area east of KASH, evident in the recent earthquake swarm of the region (Figure 2). Such an assessment is strengthened by the observation that another station, WUQI, located  $\sim 60$  km west of KASH, also moves southward (more so than KASH) relative to the stable part of the Tarim. WUQI moves  $7 \pm 2$  mm/yr  $N125^\circ \pm 16^\circ E$  relative to KASH, likely reflecting active faulting between the two sites.

At the eastern end of the Altyn Tagh fault, slightly oblique convergence of  $7 \pm 2$  mm/yr in the  $N65^\circ E$  direction is detected across the west-northwest trending Qilian Shan-Nan Shan thrust belt. Specifically, a rate of  $3 \pm 2$  mm/yr left slip motion parallel to the thrust belt and a rate of  $6 \pm 2$  mm/yr perpendicular to the thrust belt were estimated between station JIUQ in the Hexi corridor north of the thrust belt and a group of seven stations (WUTU, GELM, CHAI, A603, NUOM, DELI, and XINI) in the

central and eastern Qaidam basin (Figure 6). Southwest of the basin the Qimen Tagh fault, bending from northwest trend to west-southwest trend as it approaches the Altyn Tagh fault, does not appear to be very active. There is virtually zero convergence between station ALAE, located west of the Qimen Tagh fault, and all the sites located in the Qaidam basin east of the fault. The  $\sim 6$  mm/yr northeast-southwest convergence across the Qaidam basin and its two flanks (the Qilian Shan-Nan Shan and the Qimen Tagh thrust belts) differs from Meyer *et al.*'s [1998]  $\sim 15$  mm/yr shortening in the same direction across the region.

## 5. Discussion

### 5.1. Slip Rate Along the Altyn Tagh Fault

The slip rate along the Altyn Tagh fault is central to differentiating the discrete versus distributed deformation models for the Indo-Asian collision [e.g., Peltzer and Tapponnier, 1988; England and Houseman, 1986]. In the past decade, highly variable estimates have been obtained for the Quaternary fault slip rate along the Altyn Tagh fault. In the first systematic study using Landsat images, Peltzer *et al.* [1989] deduced a rate of  $\sim 20$  mm/yr along the Karakash and  $\sim 30$  mm/yr along the central segment of the Altyn Tagh from offset

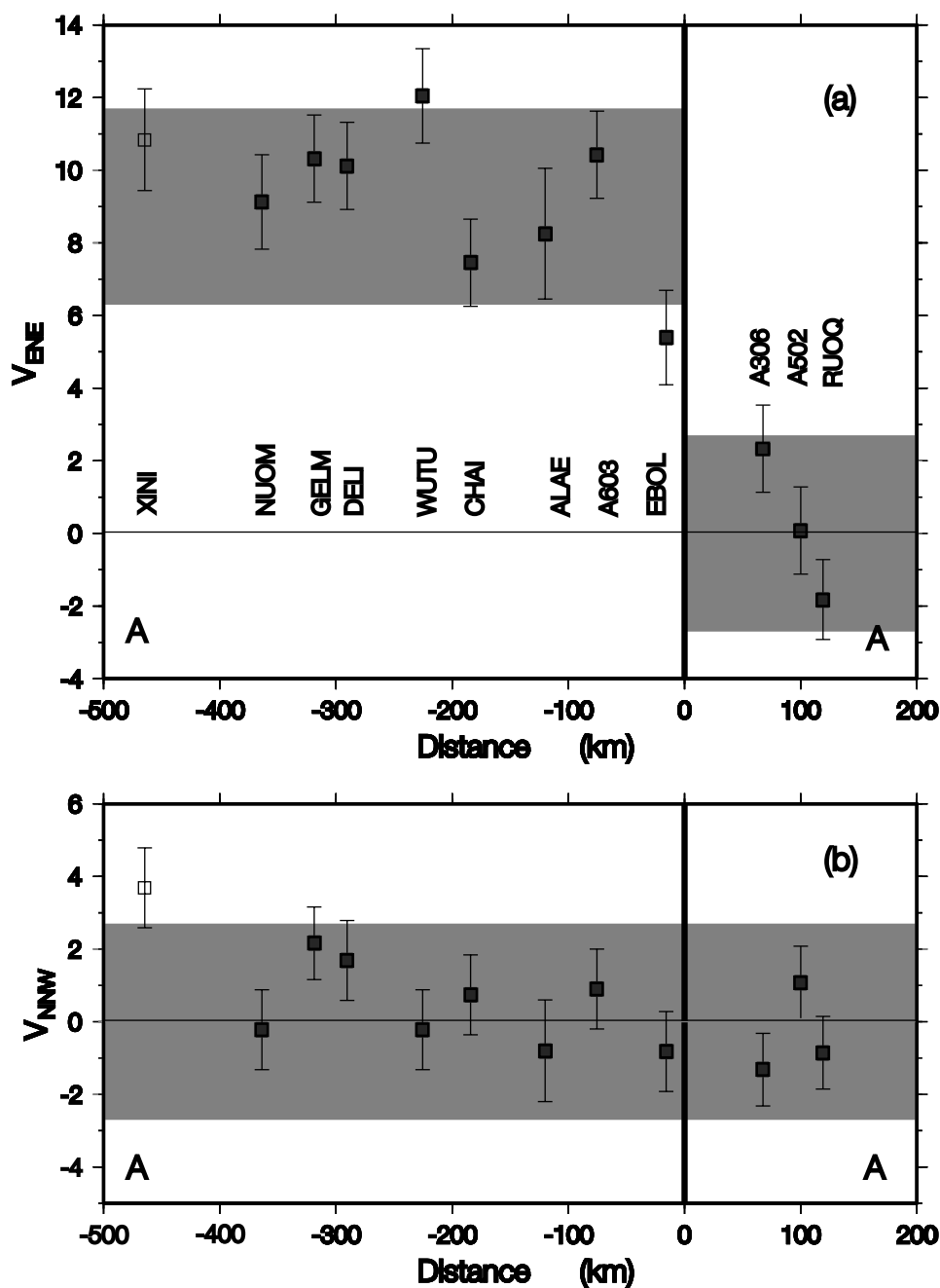


**Figure 7.** Velocity profiles across the central Altyn Tagh fault (A-A' in Figure 5). All the station velocities are referenced to the Tarim basin and projected to the fault normal direction N20°W. (a) Fault-parallel component. (b) Fault-normal component. Data are shown with 1 $\sigma$  standard deviation. Vertical bar denotes the location of the southern branch of the Altyn Tagh fault. Here  $9 \pm 2$  mm/yr left slip and  $0 \pm 2$  mm/yr normal motion across the fault are derived. The apparent anomaly for the fault-normal component of station XINI is partially due to the distortion of a planar projection of a spherical surface.

geomorphic features across the fault, assuming the features were formed since the Last Glacial Maximum. *Avouac and Tapponnier* [1993] used this high slip rate to support a microplate model for the Indo-Asian collision zone. More recent studies based on offsets of geomorphic features and cosmogenic dating also supported the rate of  $\sim 20$  mm/yr along the Karakash [*Ryerson et al.*, 1999] and 20–30 mm/yr along the central segment of the Altyn Tagh [*Meriaux et al.*, 2000]. On the other hand, surface mapping, trenching across the

active trace of the Altyn Tagh fault, and  $^{14}\text{C}$  dating by a Chinese research group placed a minimum constraint on the Quaternary slip rate at  $\sim 5$  mm/yr over the entire length of the Altyn Tagh fault [*SSBC*, 1992].

*England and Molnar* [1997] used estimated slip rates along other major active faults in the Indo-Asian collision zone to determine the range of slip rates along the Altyn Tagh fault consistent with the regional strain pattern. Employing a finite element scheme under strain compatibility constraints, they found that only when the

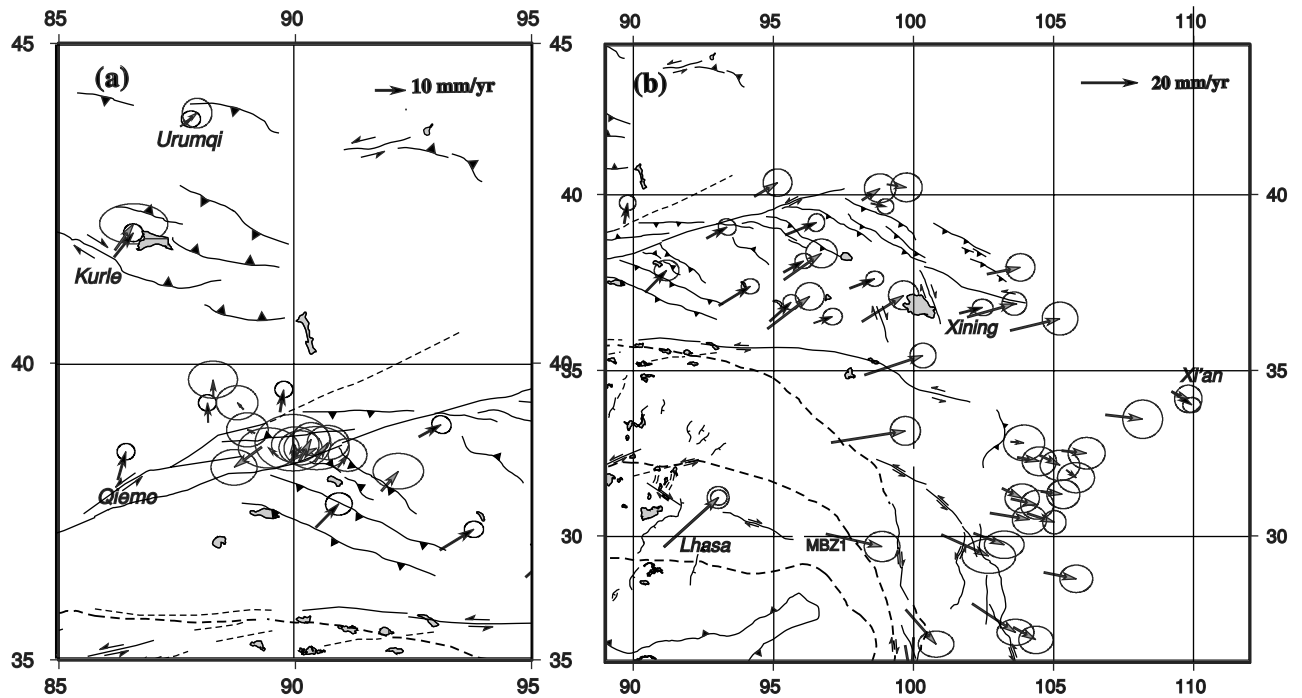


**Figure 8.** Comparisons of GPS velocity results. (a) Comparison of our results (solid arrows) with that of *Bendick et al.* [2000] (shaded arrows) at the central Altyn Tagh. *Bendick et al.*'s velocities have been rotated to align with our reference frame using collocated site velocities at Kurler and Urumqi. Error ellipses represent 95% confidence level. The two studies show a good agreement on the deformation pattern across the central Altyn Tagh fault. (b) Comparison of our results (solid arrows) with that of *Chen et al.* [2000] (shaded arrows) at northeast Tibet. A minor rotation of *Chen et al.*'s velocities (based on 13 common IGS stations in the Eurasia plate) is performed to align the two sets of velocities to a common reference frame. A systematic mismatch of the eastward motion between the two sets of solutions is found. See text for detailed discussions.

Altyn Tagh fault moves at a rate of  $\sim 10$  mm/yr would the regional strain data be explained. Because this test assumed slip rates on other Cenozoic faults in Asia which were perhaps even more poorly determined, the result is far from conclusive.

*Bendick et al.* [2000] measured a low slip rate of  $9 \pm 5$  mm/yr across the central part of the Altyn Tagh fault using GPS along approximately the section shown in our Figure 7. Their data showed some heterogeneity within the Altyn Tagh range, but their result is generally consistent with ours along the same section of the fault (Figure 8a). *Chen et al.* [2000] reported rates of  $6 \pm 2$  mm/yr and  $9 \pm 2$  mm/yr on two lines straddling the fault near longitude  $95^\circ\text{E}$ . We made no measurements north of the Altyn Tagh fault between  $90^\circ$  and  $98^\circ\text{E}$ , so their data provide an important complement to ours. The combined data show low slip rates,  $< 11$  mm/yr, on the central and eastern Altyn Tagh fault. The result also suggests that only minor deformation exists between the Tarim basin and the region northeast of the Qilian Shan (Figure 5). For example, station JIUQ moves at only  $\sim 3$  mm/yr relative to three sites 800 km west of JIUQ and north of the Altyn Tagh range. Our slip rate estimate at the central Altyn Tagh could be as much as 11 mm/yr if we take the rate at RUOQ (the site farthest from the fault, Figure 7) as representative of the Tarim block. The rate, however, could not be much higher than this because it would contradict the velocities of other sites within the Tarim basin.

The discrepancy between the geodetic and geological estimates of slip rate along the Altyn Tagh fault is a real puzzle. The low geodetic rate ( $\sim 10$  mm/yr) cannot be attributed to near-fault locking because our GPS network spans several hundred kilometers across the fault. If both geodetic and

geological results are correct, the discrepancy must be explained by spatial or temporal differences in the two types of measurement.

We may first consider the spatial differences between geological and GPS measurements. For the Karakash fault the geological [*Peltzer et al.*, 1989] and geodetic (this study) measurements were made approximately along the same section of the fault. For the central section of the Altyn Tagh the geological measurements were made at  $\sim 88^\circ\text{E}$ , and our GPS were at  $\sim 90^\circ\text{E}$ . We have no GPS estimate of slip rate along the Altyn Tagh fault system from  $80^\circ$  to  $90^\circ\text{E}$ . Nevertheless, our GPS results suggest an upper bound for the current slip rate on that segment. If the Altyn Tagh fault moves at a rate of 20–30 mm/yr along its central segment, one would expect a significant convergence in the ENE-WSW direction across the Qimen Tagh thrust belt at the southern margin of the Qaidam basin (Figure 1). However, this is not supported by our result across the fault. Since there is no known active thrust fault west of the Qimen Tagh and south of the active trace of the Altyn Tagh fault, the current slip rate along the Altyn Tagh fault must be about the same from the Qaidam segment to the Karakash valley segment. This result implies that the Tibetan plateau just south of the Altyn Tagh between  $80^\circ$  and  $92^\circ\text{E}$  behaves more or less like a rigid block, and the slip rate discrepancy cannot be explained by the location difference of the two types of the measurements.

Could different timescales explain the discrepancy between geodetic and geologic results? We do not yet know any mechanism that would reduce a long-term average slip rate of  $> 20$  mm/yr to half or less measured during a period of a few years.

Earthquake stress may accelerate the deformation near the rupture zone, so that long after a large earthquake, the strain rate may be lower than average. Also, most of the Altyn Tagh fault has not been ruptured for more than a century. However, the geodetic data cover a wide zone, and they should be relatively insensitive to deformation from individual earthquakes. If earthquakes are responsible for the longer-term geologic slip rate, then they must have occurred on the Altyn Tagh fault at a phenomenal rate in the past. Intensive efforts to date Quaternary slip rates along the Altyn Tagh fault are currently underway [Washburn *et al.*, 2000; Meriaux *et al.*, 2000]. Only when the slip rate history of the Altyn Tagh fault is determined at various timescales from several years to several millions of years can we confidently test the long-term role of the Altyn Tagh fault in the Indo-Asian collision tectonics.

The Altyn Tagh fault system has long been viewed as a transpressional system which partitions both the left slip motion along the Altyn Tagh fault and fault-perpendicular shortening across the North Altyn Tagh fault [Burchfiel *et al.*, 1989; Wittlinger *et al.*, 1998]. For example, England and Molnar [1997] estimated a shortening rate of  $6 \pm 4$  mm/yr across the central section of the Altyn Tagh fault. Bendick *et al.* [2000] reported a contraction rate of  $3 \pm 1$  mm/yr across the same section. Chen *et al.* [2000] estimated  $5 \pm 2$  mm/yr across the east section at  $\sim 95^\circ\text{E}$ . In contrast to these early inferences, geologic mapping along the North Altyn Tagh fault by Cowgill *et al.* [2000] suggested that it is mostly a left slip fault with only minor compression. Although our result of  $0 \pm 2$  mm/yr convergence across the central Altyn Tagh system is within the range of uncertainty of Bendick *et al.*'s [2000] estimate of  $3 \pm 1$  mm/yr, it indicates strongly that north-south shortening across the Altyn Tagh system is negligible. To the west our  $\sim 2$  mm/yr shortening across the Western Kunlun thrust belt at  $\sim 80^\circ\text{E}$  is also at odds with a geological finding of  $\sim 8$  mm/yr by Lyon-Caen and Molnar [1984] and by Avouac and Tapponnier [1993]. The discrepancy between various geological and geodetic results for the fault shortening rate is another mystery and invites further investigation.

At the easternmost end of the Altyn Tagh fault, Meyer *et al.* [1996] estimated a slip rate of  $4 \pm 2$  mm/yr, and Peltzer *et al.* [1989] suggested  $\sim 5$  mm/yr for a splay emanating from the Altyn Tagh fault and curving into the Qilian Shan frontal thrust. Our value of  $\sim 9$  mm/yr is significantly higher than their estimates. We attribute the difference to the fact that our rate is measured along the Altyn Tagh system to the west where only a single strand is active, whereas the region studied by Peltzer *et al.* [1989] and Meyer *et al.* [1996] is characterized by multiple strands of active faults splaying into the Qilian Shan-Nan Shan thrust belt. Despite the lack of details on the deformation field at the eastern end of the Altyn Tagh fault our result places a bound of convergence across the Qilian Shan-Nan Shan thrust belt at  $6 \pm 2$  mm/yr. This rate is lower than the  $10 \pm 3$  mm/yr estimate of Chen *et al.* [2000], but the two results overlap at the 95% confidence level.

## 5.2. Eastward Motion of Tibet

Our result not only constrains the kinematics of the Altyn Tagh fault system but also has implications for the overall deformation pattern between central Tibet and the Tian Shan. In particular, our GPS results imply that the Qaidam-Kunlun block in northern Tibet coherently moves east-northeastward at a rate of  $\sim 8$  mm/yr with respect to Tarim as well as Siberia. We also detect  $\sim 6$  mm/yr eastward motion for the region between the Karakash fault in the north and the Longmu-Gozha Co fault in the south.

Although our result of east-northeastward motion for northeast Tibet with respect to Siberia qualitatively agrees with that of Chen *et al.* [2000], we disagree quantitatively. Our result yields  $\sim 9$  mm/yr eastward motion for the Qaidam basin sites with respect to Siberia from our EURASIA solution (Table 2, Regional Station

Velocities), while Chen *et al.* [2000] estimated  $\sim 15$  mm/yr for the sites in the same region from their "Eurasia" solution (Figure 8b). The discrepancy cannot be fully explained by the reference frame difference since the two reference frames were derived using almost the same strategy and nearly the same set of IGS stations. The offsets between the two results at SHAO, XIAN, and WUHN, all in east Asia, are  $\sim 1$  mm/yr or less. The velocity of Chen *et al.* [2000] for northeast Tibet, however, was based on data from only two epochs, and the first of these (June–July 1996) coincided with excursions in their time series for the east positions of LHAS and XIAN that suggest regionally correlated errors (R. King, personal communication, 2001).

The  $\sim 6$  mm/yr discrepancy has strong implications for tectonics in the eastern Tibetan plateau and its borderland. For example, Chen *et al.* [2000] hypothesized that the motion of Tibet to the east might be absorbed by thrusts and folds in the Liupan Shan and Mibo Shan [Zhang *et al.*, 1990, 1991]. They also inferred 8–10 mm/yr right shear motion across faults trending northeast between the northeast Tibet and the Longmen Shan. According to our study, however, if such thrust and shear motions occur at the eastern borderland of Tibet, they could not exceed 4 mm/yr. In contrast to  $\sim 10$  mm/yr eastward motion of Chen *et al.* [2000] for the region north of the Altyn Tagh fault with respect to Siberia, our result shows virtually zero eastward motion. We conclude that north-south crustal thickening across Tian Shan is the major mechanism to accommodate the northward indentation north of the Altyn Tagh fault.

The slower eastward motion ( $\sim 8$  mm/yr) of the Qaidam-Kunlun block obtained by this study contrasts with a fast eastward motion of south central Tibet based on GPS and geological studies [e.g., Larson *et al.*, 1999; Yin and Harrison, 2000]. For example, in this study, station LHAS moves  $\sim 21$  mm/yr eastward with respect to Siberia, which is probably accommodated by a series of north-south trending rifts in Tibet located both north and south of the Bangong-Nujiang suture west of the site [Yin *et al.*, 1999; Yin, 2000; Larson *et al.*, 1999; Freymueller *et al.*, 1999]. This motion is  $\sim 13$  mm/yr faster than sites located in the Qaidam basin (Tables 1 and 2). Such differential motion of 13 mm/yr is probably accommodated mainly along the Kunlun fault. This inference is consistent with the results of geological studies by Kidd and Molnar [1988] and by Van der Woerd *et al.* [1998], who reported a slip rate of  $\sim 13$  mm/yr on the fault.

How the left slip Kunlun fault terminates at its western end remains unclear, as the trace of the fault becomes obscured west of  $90^\circ\text{E}$ . Analysis of Landsat images and fault plane solutions suggested that the Kunlun fault branches off westward into several ENE trending left slip fault splays [Tapponnier and Molnar, 1977; Armijo *et al.*, 1986, 1989; Molnar and Lyon-Caen, 1989]. The 1997 Manyi earthquake of  $M = 7.6$  occurred on one of these left slip faults [Peltzer *et al.*, 1999; Velasco *et al.*, 2000]. Two  $M = 6$  events also occurred in the same region in 1985 with similar focal mechanisms and possibly on the same fault segment [Ekstrom and England, 1989]. In return, these nearly east-west trending left slip faults at the western end of the Kunlun fault are probably linked with a series of rifts and faults. They include north-south trending rifts in central Tibet between the Jinsha and Bangong-Nujiang sutures and the normal and strike-slip faults in the western Qiangtang block [Yin *et al.*, 1999; Tapponnier and Molnar, 1977; M. H. Taylor *et al.*, Distributed eastward extrusion of central Tibet: A new perspective from geologic studies of rift-bounding faults in north Tibet, submitted to Tectonics, 2001 (hereinafter Taylor *et al.*, submitted manuscript, 2001)]. This system probably extends westward to the Longmu-Gozha Co but not the Karakash fault [Avouac, 1991; Peltzer *et al.*, 1989], however, because our result shows that the region south of the Karakash fault and north of the Longmu-Gozha Co and Kunlun faults moves almost coherently eastward only 2–3 mm/yr slower than the Qaidam block.

### 5.3. Deformation in the Western Kunlun Shan Region

The Western Kunlun thrust belt and the Karakash fault separate the Pamir plateau in the west from the Tarim basin in the east. Tectonic deformation in the region is extremely complex. The convergence rate across the western Kunlun thrust belt seems to increase westward, as the system bends northward from nearly east-west strike to NNW-SSE strike. This systematic increase in convergence rate was first speculated by *Rumelhart et al.* [1999] on the basis of preliminary paleomagnetic results. GPS confirmation of the westward increase in convergent rate implies that the western Kunlun Shan in the hanging wall of the western Kunlun thrust belt rotates clockwise with respect to the Tarim basin. This behavior may result from oroclinal bending due to northward indentation of the Pamir syntaxis into Asia [*Burtman and Molnar, 1993; Rumelhart et al., 1999*]. In addition, a component of range-parallel (WNW-ESE) shortening occurs between stations TAHE and A105 at a rate of  $\sim 10$  mm/yr within the western Kunlun. Such shortening may be accommodated by diffuse left slip shearing in the region between the two stations, caused by "bookshelf" style shear and clockwise rotation around the Tarim block, like the deformation pattern in the western Transverse Ranges of the western United States [*Luyendyk, 1991*]. The northeast Pamir experiences east-west extension as expressed by active normal faulting along the north-south trending Kongur Shan normal fault system [*Brunel et al., 1994*]. Just east of the normal fault, there is  $\sim 7$  mm/yr east-west shortening between TAHE and SHAC straddling two possible thrust faults. Perhaps the contraction to the east results from subduction of the western Tarim basin, while the extension to the west results from flexure of the hanging wall.

### 5.4. Surface Area Balance

Despite the uncertainties and still limited spatial coverage associated with our GPS data a preliminary inference can be made about the deformation style based on results of this and previous GPS studies in and around the Tibetan plateau. A recently revised plate motion model suggested a current convergence rate between India and Siberia, projected across the Himalaya range, as only 36–40 mm/yr, significantly slower than that determined by the NUVEL-1 model [*Gordon et al., 1999*]. This result has also been supported by recent GPS estimates [*Shen et al., 2000; Chen et al., 2000*]. Using the Indo-Asian convergence rate and GPS-derived deformation rates around the Tibetan plateau, we may assess quantitatively how the Indo-Eurasia convergence is accommodated in Asia. Assuming an India-Tibet plate boundary of  $\sim 2400$  km long and an average convergence rate of  $\sim 38$  mm/yr, the total area reduction between the two plates would be  $\sim 0.091$  km<sup>2</sup>/yr projected at the Himalaya. Northeast of the Tibetan plateau, a rigid body eastward motion of the Qaidam-Kunlun Shan block with respect to Siberia at the rate of 9 mm/yr would move  $\sim 0.005$  km<sup>2</sup>/yr surface area out of the region. South of the Kunlun fault the eastward motion of the Tibetan plateau would accommodate  $\sim 0.016$  km<sup>2</sup>/yr surface area reduction, assuming an average eastward motion rate of  $\sim 20$  mm/yr with respect to Siberia across a north-south trending profile of 800 km wide. This result is based on the assumption that the station velocity of BMZ1 of *Chen et al.* [2000] is representative of the regional deformation rate. Thus the total eastward extrusion would account for  $\sim 0.021$  km<sup>2</sup>/yr:  $\sim 23\%$  of the total surface area reduction due to Indo-Asia collision. North of the Tarim basin our result suggests that crustal shortening in the Tian Shan range consumes  $\sim 0.017$  km<sup>2</sup>/yr surface area:  $\sim 19\%$  of the total surface area reduction due to Indo-Asia collision. The shortening across the Himalaya thrust belt is  $\sim 20$  mm/yr [*Bilham et al., 1997; Larson et al., 1999*], which is equivalent to  $\sim 53\%$  of the total surface area

reduction. As a result, there is an insignificant amount of the Indo-Eurasia convergence left to be accommodated by other mechanisms, such as gross thickening of the plateau crust. We still do not know how much shear and normal faulting is taking place in central and southern Tibet. Nevertheless, first-order deformation in Tibet seems mainly controlled by deformation along a few major faults and within several thrust belts such as the Himalaya and the Tian Shan.

## 6. Conclusions

The central section of the Altyn Tagh fault slips at a slow rate of  $9 \pm 2$  mm/yr, and the Karakash fault slips at a rate of  $7 \pm 3$  mm/yr. The convergence rates across the faults are also small,  $0 \pm 2$  mm/yr across the central section of the Altyn Tagh and  $2 \pm 2$  mm/yr across the Karakash. Between the central section of the Altyn Tagh and the Karakash ( $80^\circ$ – $90^\circ$ E) the fault is likely to slip at a rate of  $\sim 10$  mm/yr as well.

Deformation of the Tarim and Qaidam basins can be described by rigid block motion. In particular, the Tarim and Qaidam basins rotate clockwise with respect to Siberia at rates of  $\sim 11$  and 4.5 nrad/yr, respectively. The region just south of the Altyn Tagh fault and north of the Kunlun fault-western Jinsha suture may be part of the Qaidam-Kunlun rigid block.

North-south convergence across the central Tian Shan ( $77^\circ$ E) is  $\sim 18$  mm/yr and across the eastern Tian Shan ( $87^\circ$ E) is  $\sim 6$  mm/yr. There is little east-west shear motion along the Tian Shan southern frontal fault system.

The Kashgar region, located at the westernmost tip of the Tarim basin, moves  $7 \pm 2$  mm/yr southward with respect to the interior of the Tarim block, suggesting that either the region is part of the active southern Tian Shan deformation zone or significant elastic strain is accumulating along the southern Tian Shan thrust belt.

Crustal deformation of the western Kunlun Shan is the result of multiple tectonic processes. Its east-west contraction suggests westward subduction of the Tarim block; the normal faulting west of the contraction zone implies flexure of the hanging wall, and its clockwise rotation and left-lateral shear seem to be the result of northward indentation of the Pamir and westward subduction of the Tarim.

Northernmost Tibet moves  $\sim 8$  mm/yr eastward, and the Tarim basin shows no detectable motion with respect to Siberia. The eastward motion of the Tibetan plateau currently accommodates  $\sim 23\%$ , the Tian Shan system accommodates  $\sim 19\%$ , and the Himalaya thrust belt accommodates  $\sim 53\%$  of the Indo-Asia convergence. These three tectonic elements account for  $\sim 95\%$  of the Indo-Asia relative plate motion.

**Acknowledgments.** Chengkun Zhao processed part of the GPS data during the early stage of this study. We thank IGS and its east and central Asia members for providing their GPS data. Discussions with Eric Cowgill and Mike Murphy and comments by Bob King, Ramon Arrowsmith, and Zack Washburn are appreciated. We are grateful to Kathy Jackson for help on writing. We also thank Mike Taylor for providing his Tibetan fault database. Critical reviews by Peter Molnar, Barry Parsons, and an anonymous reviewer helped improved the manuscript. Figures were produced using the GMT software [*Wessel and Smith, 1995*]. This research was supported by NSF grants EAR9725599 from the Continental Dynamics Program and EAR9805010 and EAR99903143 from the Geophysics Program, and by PRC Ministry of Science and Technology grant of G1998007 from the Major Science Advancement Program.

## References

- Abdrakhmatov, K. Y., et al., Relatively recent construction of the Tien Shan inferred from GPS measurements of present-day crustal deformation rates, *Nature*, 384, 450–453, 1996.
- Abe, K., Magnitudes of large shallow earthquakes from 1904 to 1980, *Phys. Earth Planet Inter.*, 34, 17–23, 1984.
- Allen, M. B., S. J. Vincent, and P. J. Wheeler, Late Cenozoic tectonics of

- the Kepingtage thrust zone: Interactions of the Tien Shan and Tarim Basin, northwest China, *Tectonics*, **18**, 639–654, 1999.
- Argus, D. F., and R. G. Gordon, No-net-rotation model of current plate velocities incorporating plate motion model NUVEL-1, *Geophys. Res. Lett.*, **18**, 2039–2042, 1991.
- Armijo, R., P. Tapponnier, J. L. Mercier, and T. Han, Quaternary extension in southern Tibet: Field observations and tectonic implications, *J. Geophys. Res.*, **91**, 13,803–13,872, 1986.
- Armijo, R., P. Tapponnier, and T. Han, Late Cenozoic right-lateral strike-slip faulting in southern Tibet, *J. Geophys. Res.*, **94**, 2787–2838, 1989.
- Avouac, J.-P., Application des methodes de morphologie quantitative a la neotectonique, Modele cinematique des deformations actives en Asie Centrale, Ph.D. thesis, Univ. Paris VII, Paris, 1991.
- Avouac, J.-P., and G. Peltzer, Active tectonics in southern Xinjiang, China: Analysis of terrace riser and normal fault scarp degradation along the Hotan-Qira fault system, *J. Geophys. Res.*, **98**, 21,773–21,807, 1993.
- Avouac, J.-P., and P. Tapponnier, Kinematic model of active deformation in central Asia, *Geophys. Res. Lett.*, **20**, 895–898, 1993.
- Bendick, R., R. Bilham, J. Freymueller, K. Larson, and G. Yin, Geodetic evidence for a low slip rate in the Altyn Tagh fault system, *Nature*, **404**, 69–72, 2000.
- Bilham, R., K. Larson, and J. Freymueller, GPS measurements of present-day convergence across the Nepal Himalaya, *Nature*, **386**, 61–64, 1997.
- Bird, P., and K. Piper, Plane-stress finite-element models of tectonic flow in southern California, *Phys. Earth Planet Inter.*, **21**, 158–175, 1981.
- Bock, Y., et al., Southern California Permanent GPS Geodetic Array: Continuous measurements of regional crustal deformation between the 1992 Landers and 1994 Northridge earthquakes, *J. Geophys. Res.*, **102**, 18,013–18,033, 1997.
- Brunel, M., N. Arnaud, P. Tapponnier, Y. Pan, and Y. Wang, Kongur Shan normal fault: Type example of mountain building assisted by extension (Karakorum fault, eastern Pamir), *Geology*, **22**, 707–710, 1994.
- Burchfiel, B. C., Q. Deng, P. Molnar, L. H. Royden, Y. Wang, P. Zhang, and W. Zhang, Intracrustal detachment with zones of continental deformation, *Geology*, **17**, 752–784, 1989.
- Burchfiel, B. C., E. T. Brown, Q. D. Deng, X. Y. Feng, J. Li, P. Molnar, J. B. Shi, Z. M. Wu, and H. C. You, Crustal shortening on the margins of the Tien Shan, Xinjiang, China, *Int. Geol. Rev.*, **41**, 665–700, 1999.
- Burtman, V. S., and P. Molnar, Geological and geophysical evidence for deep subduction of continental crust beneath the Pamir, *Spec. Pap. Geol. Soc. Am.*, **281**, 1993.
- Chen, Z., B. C. Burchfiel, Y. Liu, R. W. King, L. H. Royden, W. Tang, E. Wang, J. Zhao, and X. Zhang, Global Positioning System measurements from eastern Tibet and their implications for India/Eurasia intercontinental deformation, *J. Geophys. Res.*, **105**, 16,215–16,227, 2000.
- Cowgill, E., A. Yin, X. F. Wang, and Q. Zhang, Is the North Altyn fault part of a strike-slip duplex along the Altyn Tagh fault system?, *Geology*, **28**, 255–258, 2000.
- DeMets, C., R. G. Gordon, D. F. Argus, and S. Stein, Current plate motions, *Geophys. J. Int.*, **101**, 425–478, 1990.
- DeMets, C., R. G. Gordon, D. F. Argus, and S. Stein, Effect of recent revisions to the geomagnetic reversal time scale on estimates of current plate motions, *Geophys. Res. Lett.*, **21**, 2191–2194, 1994.
- Dewey, J. F., and K. Burke, Tibetan, Variscan and Precambrian basement reactivation: Products of continental collision, *J. Geol.*, **81**, 683–692, 1973.
- Dong, D., T. A. Herring, and R. W. King, Estimating regional deformation from a combination of space and terrestrial geodetic data, *J. Geod.*, **72**, 200–214, 1998.
- Ekstrom, G., and P. England, Seismic strain rates in regions of distributed continental deformation, *J. Geophys. Res.*, **94**, 10,231–10,257, 1989.
- England, P. C., and G. A. Houseman, Finite strain calculations of continental deformation, 2, Comparison with the India-Asia collision zone, *J. Geophys. Res.*, **91**, 3664–3676, 1986.
- England, P., and P. Molnar, The field of crustal velocity in Asia calculated from Quaternary rates of slip on faults, *Geophys. J. Int.*, **130**, 551–582, 1997.
- Freymueller, J. T., Q. Chen, Q. Wang, Z. Yang, W. Wang, K. M. Larson, R. Bilham, R. Bendick, and H. Fletcher, Present-day kinematics of the India-Eurasia plate collision zone, *Eos Trans. AGU*, **80**(46), Fall Meet. Suppl., F1022, 1999.
- Gordon, R. G., D. F. Argus, and M. B. Heflin, Revised estimate of the angular velocity of India relative to Eurasia (abstract), *Eos Trans. AGU*, **80**(46), Fall Meet. Suppl., F273, 1999.
- Herring, T. A., GLOBK: Global Kalman filter VLBI and GPS analysis program, version 4.0, Mass. Inst. of Technol., Cambridge, 1995.
- Holt, W. E., M. Li, and A. J. Haines, Earthquake strain rates and instantaneous relative motions within central and eastern Asia, *Geophys. J. Int.*, **122**, 569–593, 1995.
- Holt, W. E., N. Chamot-Rooke, X. Le Pichon, A. J. Haines, B. Shen-Tu, and J. Ren, The velocity field in Asia inferred from Quaternary fault slip rates and Global Positioning System observations, *J. Geophys. Res.*, **105**, 19,185–19,209, 2000.
- Houseman, G. A., and P. C. England, A lithospheric thickening model for the Indo-Asian collision, in *The Tectonics of Asia*, edited by A. Yin and T. M. Harrison, pp. 2–17, Cambridge Univ. Press, New York, 1996.
- Jiang, X., M. K. McNutt, and Y. Jin, Models of Lithospheric deformation beneath the Altyn Tagh and West Kunlun Faults from recent gravity surveys, *Eos Trans. AGU*, **80**(46), Fall Meet. Suppl., F1008, 1999.
- Kao, H., R. Gao, R.-J. Rau, Y. Guan, R.-Y. Chen, and D. Shi, Seismological evidence against the subduction of Tarim block beneath Tibet: Preliminary results from a broadband seismic experiment along the Tarim-Tibet Border, *Eos Trans. AGU*, **80**(46), Fall Meet. Suppl., F1008, 1999.
- Kidd, W. S. F., and P. Molnar, Quaternary and active faulting observed on the 1985 Academia Sinica-Royal Society geotraverse of Tibet, *Philos. Trans. R. Soc. London, Ser. A*, **327**, 337–363, 1988.
- King, R. W., and Y. Bock, Documentation for the MIT GPS analysis software: GAMIT, version 9.3, Mass. Inst. of Technol., Cambridge, 1995.
- King, R. W., F. Shen, B. C. Burchfiel, L. H. Royden, E. Wang, Z. Chen, Y. Liu, X.-Y. Zhang, J.-X. Zhao, and Y. Li, Geodetic measurement of crustal motion in southwest China, *Geology*, **25**, 179–182, 1997.
- Kogan, M. G., G. M. Steblov, R. W. King, T. A. Herring, D. I. Frolov, S. G. Egorov, V. Y. Levin, A. Lerner-Lam, and A. Jones, Geodetic constraints on the rigidity and relative motion of Eurasia and North America, *Geophys. Res. Lett.*, **27**, 2041–2044, 2000.
- Kong, X., and P. Bird, Neotectonics of Asia: Thin-shell finite-element models with faults, in *Tectonic Evolution of Asia*, edited by A. Yin and T. M. Harrison, pp. 18–34, Cambridge Univ. Press, New York, 1996.
- Larson, K. M., J. T. Freymueller, and S. Philipson, Global plate velocities from the Global Positioning System, *J. Geophys. Res.*, **102**, 9961–9981, 1997.
- Larson, K. M., R. Burgmann, R. Bilham, and J. T. Freymueller, Kinematics of the India-Eurasia collision zone from GPS measurements, *J. Geophys. Res.*, **104**, 1077–1093, 1999.
- Leloup, P. H., R. Lacassin, P. Tapponnier, D. Zhong, X. Lui, L. Zhang, and S. Ji, Kinematics of Tertiary left-lateral shearing at the lithospheric-scale in the Ailao Shan-Red River shear zone (Yunnan, China), *Tectonophysics*, **251**, 3–84, 1995.
- Luyendyk, B. P., A model for Neogene crustal rotations, transtension, and transpression in southern California, *Geol. Soc. Am. Bull.*, **103**, 1528–1536, 1991.
- Lyon-Caen, H., and P. Molnar, Gravity anomalies and the structure of western Tibet and the southern Tarim Basin, *Geophys. Res. Lett.*, **11**, 1251–1254, 1984.
- Ma, X., *Lithospheric Dynamics Atlas of China*, China Cartogr. Publ. House, Beijing, 1989.
- Meriaux, A. S., P. Tapponnier, F. J. Ryerson, X. W. Xu, F. Wang, and J. Van der Woerd, Large scale strain patterns, great earthquake breaks, and late Pleistocene slip-rate along the Altyn Tagh fault (China), paper presented at 15th Himalaya-Karakorum-Tibet Workshop, Chengdu Univ. of Sci. and Technol., Kloster Ettal, Germany, 2000.
- Meyer, B., P. Tapponnier, Y. Gaudemer, G. Peltzer, S. Guo, and Z. Chen, Rate of left-lateral movement along the easternmost segment of the Altyn Tagh Fault, east of 96°E (China), *Geophys. J. Int.*, **124**, 29–44, 1996.
- Meyer, B., P. Tapponnier, L. Bourjot, F. Metivier, Y. Gaudemer, G. Peltzer, S. Guo, and Z. Chen, Crustal thickening in Gansu-Qinghai, lithospheric mantle subduction, and oblique, strike-skip controlled growth of the Tibet plateau, *Geophys. J. Int.*, **135**, 1–47, 1998.
- Molnar, P., and H. Lyon-Caen, Fault plane solutions of earthquakes and active tectonics of the northern and eastern parts of the Tibetan Plateau, *Geophys. J. Int.*, **99**, 123–153, 1989.
- Molnar, P., and P. Tapponnier, Cenozoic tectonics of Asia: Effects of a continental collision, *Science*, **189**, 419–426, 1975.
- Peltzer, G., and F. Saucier, Present-day kinematics of Asia derived from geologic fault rates, *J. Geophys. Res.*, **101**, 27,943–27,956, 1996.
- Peltzer, G., and P. Tapponnier, Formation and evolution of strike-slip faults, rifts, and basins during the India-Asia collision: An experimental approach, *J. Geophys. Res.*, **93**, 15,085–15,117, 1988.
- Peltzer, G., P. Tapponnier, and R. Armijo, Magnitude of late Quaternary left-lateral displacements along the north edge of Tibet, *Science*, **246**, 1285–1289, 1989.
- Peltzer, G., F. Crampe, and G. King, Evidence of nonlinear elasticity of the crust from the Mw7.6 Manyi (Tibet) earthquake, *Science*, **286**, 272–276, 1999.
- Royden, L. H., B. C. Burchfiel, R. W. King, E. Wang, Z. Chen, F. Shen, and Y. Liu, Surface deformation and lower crustal flow in eastern Tibet, *Science*, **276**, 788–790, 1997.
- Rumelhart, P. E., A. Yin, E. Cowgill, R. Butler, Q. Zhang, and X.-F. Wang, Cenozoic vertical-axis rotation of the Altyn Tagh fault system, *Geology*, **27**, 819–822, 1999.
- Ryerson, F. J., G. Peltzer, P. Tapponnier, R. C. Finkel, A. Meriaux, and M.

- W. Caffee, Slip-rates on the Karakax valley segment of the Altyn Tagh fault: Constraints from surface dating, paper presented at 14th Himalaya-Karakorum-Tibet Workshop, Univ. of Potsdam, Kloster Ettal, Germany, 1999.
- Shen, Z.-K., C. Zhao, Y. Li, D. Jackson, P. Fang, D. Dong, and A. Yin, Contemporary crustal deformation in east Asia constrained by global positioning system measurements, *J. Geophys. Res.*, *105*, 5721–5734, 2000.
- Sillard, P., Z. Altamimi, and C. Boucher, The ITRF96 realization and its associated velocity field, *Geophys. Res. Lett.*, *25*, 3223–3226, 1998.
- State Seismological Bureau of China (SSBC), *The Altyn Tagh Active Fault System*, 319 pp., Seismol. Publ. House, Beijing, 1992.
- Tapponnier, P., and P. Molnar, Active faulting and tectonics in China, *J. Geophys. Res.*, *82*, 2905–2930, 1977.
- Tapponnier, P., G. Peltzer, A. Y. Le Dain, R. Armijo, and P. Cobbold, Propagating extrusion tectonics in Asia: New insight from simple experiments with plasticine, *Geology*, *10*, 1339–1384, 1982.
- Tapponnier, P., et al., Active thrusting and folding in the Qi Lian Shan, and decoupling between upper crust and mantle in northeastern Tibet, *Earth Planet. Sci. Lett.*, *97*, 382–403, 1990.
- Van der Woerd, J., F. J. Ryerson, P. Tapponnier, Y. Gaudemer, R. Finkel, A. S. Meriaux, M. Caffee, G. Zhao, and Q. He, Holocene left-slip rate determined by cosmogenic surface dating on the Xidatan segment of the Kunlun Fault (Qinghai, China), *Geology*, *26*, 695–698, 1998.
- Velasco, A. A., C. J. Ammon, and S. L. Beck, Broadband source modeling of the November 8, 1997, Tibet ( $M_w = 7.5$ ) earthquake and its tectonic implications, *J. Geophys. Res.*, *105*, 28,065–28,080, 2000.
- Washburn, Z., J. R. Arrowsmith, G. Dupont-Nivet, and X. F. Wang, Earthquake geology of the central Altyn Tagh fault from Lake Wuzhuxiao ( $38.4^\circ\text{N}$ ,  $89.9^\circ\text{E}$ ) to Lapequan ( $39.1^\circ\text{N}$ ,  $92.5^\circ\text{E}$ ), China, *Eos Trans. AGU*, *81*(48), Fall Meet. Suppl., F1137, 2000.
- Weldon, R., and E. D. Humphreys, A kinematic model of southern California, *Tectonics*, *5*, 33–48, 1986.
- Wernicke, B. P., G. J. Axen, and J. K. Snow, Basin and Range extensional tectonics at the latitude of Las Vegas, Nevada, *Geol. Soc. Am. Bull.*, *100*, 1738–1757, 1988.
- Wessel, P., and W. Smith, New version of the Generic Mapping Tools released, *Eos Trans. AGU*, *76*(33), 329, 1995.
- Wittlinger, G., P. Tapponnier, G. Ooupinet, M. Jiang, D. Shi, G. Herquel, and F. Masson, Tomographic evidence for localized lithospheric shear along the Altyn Tagh fault, *Science*, *282*, 74–76, 1998.
- Yin, A., Mode of Cenozoic east-west extension in Tibet suggests a common origin of rifts in Asia during the Indo-Asian collision, *J. Geophys. Res.*, *105*, 21,745–21,759, 2000.
- Yin, A., and T. M. Harrison, Geologic evolution of the Himalayan-Tibetan orogen, *Annu. Rev. Earth Planet. Sci.*, *28*, 211–280, 2000.
- Yin, A., S. Nie, P. Craig, T. M. Harrison, X. Qian, and G. Yang, Late Cenozoic tectonic evolution of the southern Chinese Tian Shan, *Tectonics*, *17*, 1–27, 1998.
- Yin, A., P. A. Kapp, M. A. Murphy, C. E. Manning, T. M. Harrison, M. Grove, L. Ding, X.-G. Deng, and C.-M. Wu, Significant late Neogene east-west extension in northern Tibet, *Geology*, *27*, 787–790, 1999.
- Zhang, P., B. C. Burchfiel, P. Molnar, W. Zhang, D. Jiao, Q. Deng, Y. Wang, L. H. Royden, and F. Song, Late Cenozoic tectonic evolution of Ningxia Autonomous Region, China, *Geol. Soc. Am. Bull.*, *102*, 1484–1498, 1990.
- Zhang, P., B. C. Burchfiel, P. Molnar, W. Zhang, D. Jiao, Q. Deng, Y. Wang, L. Royden, and F. Song, Amount and style of late Cenozoic deformation in the Liupan Shan area, Ningxia Autonomous Region, China, *Tectonics*, *10*, 1111–1129, 1991.
- Zhu, W., et al., Crustal motion of Chinese mainland monitored by GPS, *Sci. China, Ser. D*, *43*, 394–400, 2000.

D. Dong, Jet Propulsion Laboratory, MS 238-332, 4800 Oak Grove Drive, Pasadena, CA 91109. (dong@freia.jpl.nasa.gov)

P. Fang, Scripps Institution of Oceanography, Scripps Orbit and Permanent Array Center (SOPAC), Cecil H. and Ida M. Green Institute of Geophysics and Planetary Physics, La Jolla, CA 92093-0225. (pfang@ucsd.edu)

D. D. Jackson, Z.-K. Shen, and A. Yin, Department of Earth and Space Sciences, University of California, Los Angeles, 90095-1567. (djackson@ucla.edu; zshen@ess.ucla.edu; yin@ess.ucla.edu)

Y. Li and M. Wang, First Crustal Deformation Monitoring Center, China Seismological Bureau, Hedong District, Tianjin, China. (djzl@shell.tjvan.net.cn; ckzhao@371.net)

(Received June 26, 2000; revised May 7, 2001; accepted July 25, 2001.)